CO_2 AND HYDROLOGY

SYUKURO MANABE

AND

RICHARD T. WETHERALD

Geophysical Fluid Dynamics Laboratory/NOAA
Princeton University
Princeton, New Jersey

1. INTRODUCTION

In the preceding article, Dickinson (this volume) critically reviews the current status of climate sensitivity research and identifies the issues that require emphasis in future investigations. This article presents, as an example, some of the results from the recent studies of climate sensitivity that have been conducted at the Geophysical Fluid Dynamics Laboratory (GFDL) under the leadership of Joseph Smagorinsky. More specifically, it discusses the hydrologic change of climate due to the future increase of the CO_2 concentration in the atmosphere.

It is well known that Smagorinsky (1956) pioneered the development of a numerical weather prediction model of the atmosphere that forecast precipitation. In addition, he and one of the present authors collaborated in the construction of a general circulation model (GCM) of the atmosphere in which the influence of the hydrologic cycle is taken into consideration for the first time (Manabe *et al.,* 1965). Therefore, it appears quite appropriate to discuss the hydrologic aspect of climate sensitivity studies in this volume dedicated to Smagorinsky.

It has been observed that the atmospheric concentration of carbon dioxide has been increasing steadily. According to the latest report of the U.S. National Academy of Sciences (1983), it is most likely that the atmospheric CO_2 concentration will exceed 600 ppm (the nominal doubling of the recent level) in the third quarter of the next century due mainly to the future

ADVANCES IN GEOPHYSICS, VOLUME 28A

increase in the fossil fuel combustion. Since CO_2 is almost transparent to solar radiation but strongly absorbs the terrestrial radiation around the wave length of 15 μm, it has been suggested that the increase in the concentration of CO_2 raises the atmospheric temperature [e.g., Callender (1938)]. Based on the results from climate models with wide varieties of complexity, a recent report from the U.S. National Academy of Sciences (1982) estimated that a doubling of CO_2 would cause a global surface-air warming of 3.0°C with a probable error of ±1.5°C. In addition, it suggested that this CO_2-induced warming of surface air is particularly pronounced in high latitudes during winter. The report also noted that the increase of atmospheric CO_2 not only raises the tropospheric temperature but also alters the hydrologic processes that operate in the atmosphere and at the Earth's surface.

Unfortunately, the CO_2-induced changes in hydrology as determined by numerical experiments conducted by various authors differ substantially from one another (Schlesinger, 1983; Dickinson, this volume). Since the temporal variability of hydrology in a general circulation model of climate is very large, it has been very difficult to distinguish the signal (i.e., CO_2-induced change in hydrology) from noise (i.e., natural hydrologic variability in the model). This partly accounts for the difference among the results from various studies mentioned previously.

Nevertheless, general circulation models of the atmosphere, which are currently available, can simulate gross characteristics of the global distribution of hydrologic variables, such as the rates of precipitation and runoff [see, for example, Manabe (1982)]. This encourages one to analyze the results from such a model for the study of hydrologic sensitivity of climate.

This paper represents an attempt to develop a coherent picture of CO_2-induced change in hydrology based on a series of numerical experiments that have been conducted at the Geophysical Fluid Dynamics Laboratory by use of general circulation models of climate with various complexities (Manabe and Wetherald, 1975, 1980; Manabe and Stouffer, 1979, 1980; Wetherald and Manabe, 1981; Manabe *et al.*, 1981). Special emphasis is placed on the identification and evaluation of the physical mechanisms responsible for these hydrologic changes.

2. Numerical Experiments

Although a wide variety of climate models have been used for the climate sensitivity studies conducted at the GFDL, the discussion in this article is based mainly on the results from a model in which a general circulation model of the atmosphere is coupled with a static mixed layer model of the ocean. In order to investigate how the increase in atmospheric CO_2 influ-

ences climate, two long-term integrations of a climate model are performed with normal and above-normal concentration of carbon dioxide. To facilitate the identification of the CO_2-induced change superposed on natural hydrologic fluctuation, it is assumed that the above-normal concentration has four times the normal value. This is much larger than the CO_2 concentration to be reached during the next century according to the latest projection by the U.S. National Academy of Sciences (1983). The period for the two time integrations is long enough (i.e., about 20 years) so that a model climate attains a quasi-steady state toward the end of these integrations. By comparing two model climates that emerge from these integrations one can evaluate the influence of the CO_2-increase on climate.

The basic structure of the aforementioned atmosphere–mixed layer ocean model is illustrated by the box diagram in Fig. 1. It consists of three basic components. They are (1) a general circulation model of the atmosphere, (2) a heat and water balance model over the continents, and (3) a simple model of the mixed layer ocean. The reader can refer to the paper by Manabe and Stouffer (1980) for the detailed description of the model. Nevertheless, it is worthwhile to briefly describe here the hydrologic and other parts of the model that are relevant to the discussions contained in this article.

In the atmospheric component of the model, the fluxes of solar and terrestrial radiation are computed by incorporating the effects of carbon dioxide, ozone, and water vapor. The mixing ratio of carbon dioxide is assumed to be constant everywhere. Ozone is specified as a function of latitude, height, and season. Cloud cover is prescribed to be zonally uniform and invariant with respect to season. The distribution of water vapor is determined by a prognostic scheme.

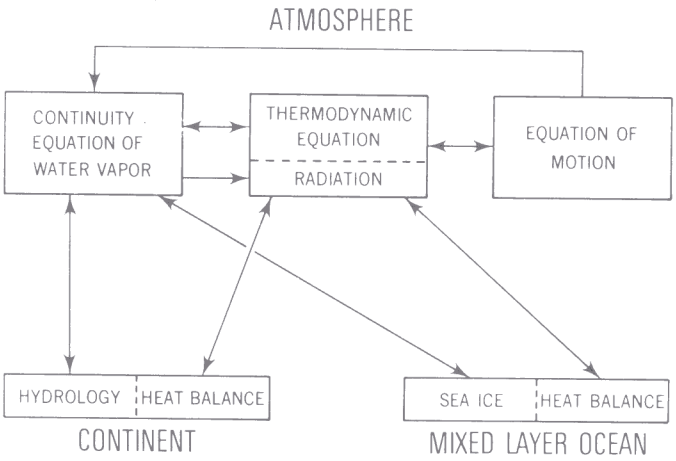

FIG. 1. Box diagram illustrating the structure of the atmosphere–mixed layer ocean model.

Precipitation is predicted wherever supersaturation is indicated by the continuity equation of water vapor. It is identified as snowfall when the air temperature near the surface falls below the freezing point. Otherwise it is identified as rainfall. The moist and dry convection are parameterized by the convective adjustment scheme as formulated by Manabe *et al.* (1965).

The temperature of the continental surface is determined so that the condition of local thermal equilibrium is satisfied among various surface heat balance components. A change in snow depth is computed as a net contribution from snowfall, sublimation, and snowmelt that is determined from the requirement of surface heat balance. High surface albedo is prescribed in snow-covered areas.

The budget of soil moisture is computed by the so-called bucket method. For the sake of simplicity, the field capacity of soil is assumed to be uniform everywhere and is 15 cm. If the soil moisture value exceeds the field capacity, runoff is predicted. A change of soil moisture is computed from the rates of rainfall, evaporation, snowmelt, and runoff. The rate of evaporation from the soil surface is determined as a function of soil moisture and the potential evaporation rate (i.e., hypothetical evaporation rate from a completely wet surface).

The oceanic component of the model is an idealized oceanic mixed layer, i.e., a well-mixed, vertically isothermal layer of sea water. For the sake of simplicity, it is assumed that the mixed layer has a uniform thickness of 68.5 m that is chosen to yield a realistic amplitude for the seasonal variation of sea-surface temperature. The change of the mixed layer temperature is computed from the budget of surface heat fluxes. The effects of horizontal heat transport by ocean currents and that of heat exchange between the mixed layer and the deeper layer of the ocean are neglected. In the presence of sea ice, the mixed layer temperature is fixed at the freezing point of sea water (i.e., $-2°C$) and the heat conduction through ice is balanced by the latent heat of freezing (or melting) at the bottom of the ice layer. This process together with the melting at the ice surface, sublimation, and snowfall determine the change in ice thickness. For the computation of net solar radiation at the oceanic surface, the albedo is prescribed as a function of latitude. Over the regions covered by sea ice, a higher value of albedo is used.

For the discussion in this article, the results from the two versions of the model are presented. The first version was originally used by Manabe and Stouffer (1980) and has a global computational domain with realistic geography. The second version was originally used by Wetherald and Manabe (1981) and has a limited computational domain with idealized geography as illustrated in Fig. 2. These two versions will be referred to as the global and sector models, respectively.

In the atmospheric component of the sector model, cyclic continuity is

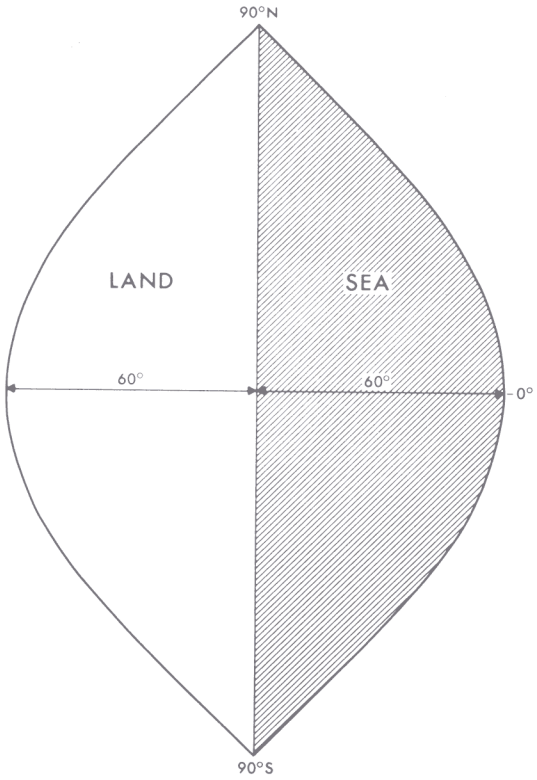

FIG. 2. Computational domain of the sector model.

assumed between the two meridional boundaries. Owing to the simplicity of its geography, this indicates the CO_2-induced climate change with a simple and broad distribution. Therefore, the results from the sector model are often very useful for the interpretation of the results from the global version of the model with more complicated, realistic geography. By seeking the common characteristics in the results from these two versions of the model, it has been possible to distinguish the signal of the CO_2-induced change from the large temporal variability of the model hydrology. Because of these reasons, the discussions in this article are conducted by comparing the results from these two versions of the model. This is essentially what Manabe *et al.* (1981) did in their study of the CO_2-induced hydrologic changes. Since the publication of their paper, it has been noted, however, that some important aspects of their results were not explained or discussed satisfactorily. This article reviews their results together with other studies from the present perspective.

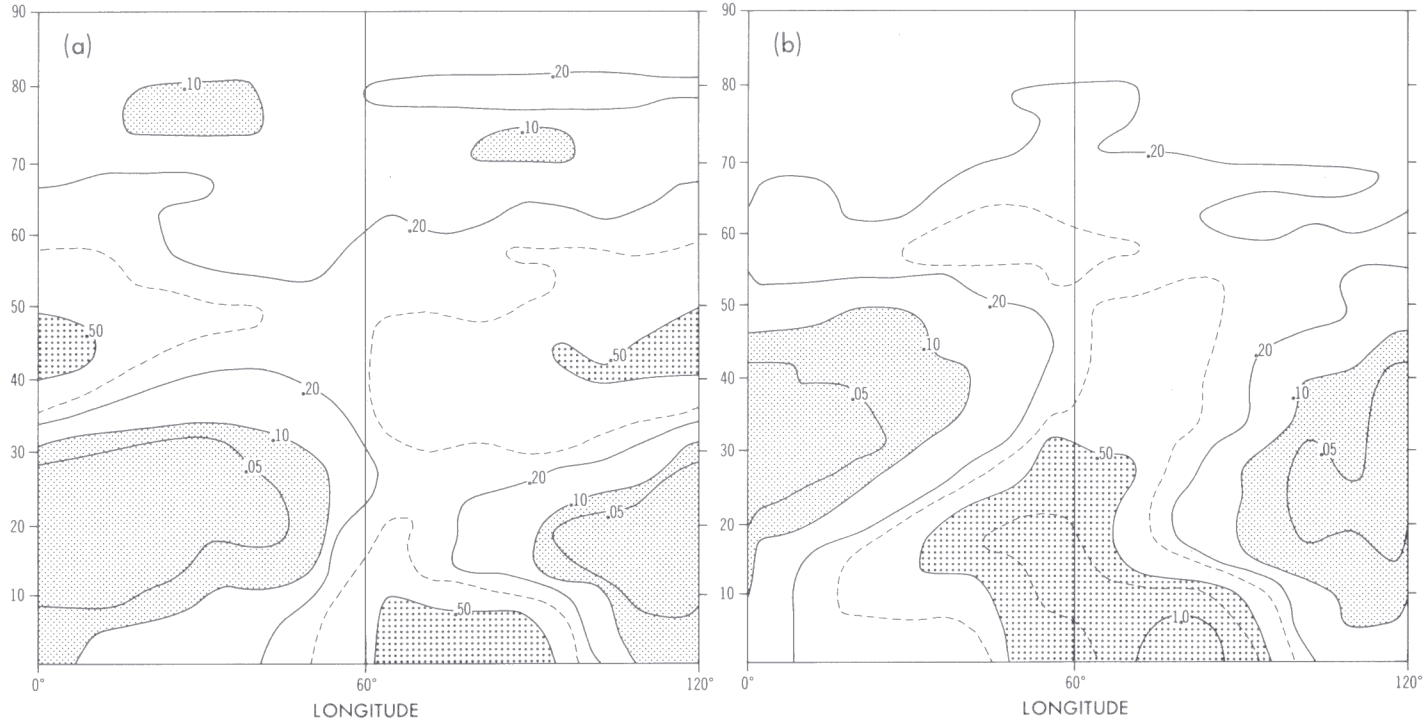

FIG. 3. Geographical distribution of 3-monthly mean rate of precipitation (centimeters per day) obtained from the sector model for (a) winter and (b) summer. The distributions of two hemispheres are averaged after shifting the phase of the seasonal variation of the Southern Hemisphere precipitation by 6 months. In both (a) and (b), the continent occupies the left half of the domain ranging from 0° to 60° longitude. [From Manabe *et al.* (1981).]

Figure 3 illustrates the geographical distributions of precipitation rate as simulated by the sector model for the winter and summer seasons. Despite its idealized geography, the sector model successfully reproduces the broad-scale features of the observed distribution of precipitation rate. For example, one can identify in the winter distribution a portion of the oceanic tropical rainbelt, a subtropical zone of minimum precipitation rate, and the middle-latitude rainbelt centered at about 45° latitude. In addition, one may note a meridional belt of relatively large precipitation rate along the east coast of subtropical part of the idealized model continent.

Turning to the summer distribution, one notes a very extensive region of intense precipitation that extends well into the continent from the western part of the tropical ocean. As compared with the winter distribution, the subtropical zone of minimum precipitation rate extends poleward accompanied by a more northward position of the middle-latitude rainbelt. These characteristics of the distribution of precipitation rate as simulated by the sector model are qualitatively similar to those of the observed precipitation rate.

One can refer to the paper by Manabe and Stouffer (1980) for the distribution of the precipitation rate from the global model with the realistic geography. Although the model distribution contains some unrealistic features, it nevertheless shares many common features with the observed distribution. The similarity between the observed and computed distributions of precipitation rate and other hydrologic variables is one of the important reasons why these models have been used for the climate sensitivity studies discussed in this article.

3. Annual Mean Response

As explained earlier, the CO_2-induced changes in hydrology are identified by comparing the two quasi-equilibrium states of a model with normal and above-normal concentrations of atmospheric carbon dioxide. One of the basic changes is the overall intensification of the hydrologic cycle. For example, the area mean rates of both precipitation and evaporation in the global model increase by as much as 7% in response to the quadrupling of atmospheric CO_2. Table I indicates the CO_2-induced percentage increase of the intensity of hydrologic cycle in various models including both the global and sector models described in this article. It clearly shows that the intensification of the hydrologic cycle occurs in a wide variety of models tabulated here.

One of the important factors responsible for the intensification of the hydrologic cycle is the change in surface radiation budget. An increase in atmospheric CO_2 enhances the downward flux of atmospheric radiation

TABLE I. PERCENTAGE INCREASE OF AREA-MEAN RATES OF PRECIPITATION (OR EVAPORATION) RESULTING FROM DOUBLING (OR QUADRUPLING) OF CO_2 CONCENTRATION IN A MODEL ATMOSPHERE[a]

Reference	Doubling (%)	Quadrupling (%)
Idealized geography		
Manabe and Wetherald (1975)[b]	7	
Manabe and Wetherald (1980)[b]	7	12
Wetherald and Manabe (1981)[b]		13
Wetherald and Manabe (1981)		10
Realistic geography		
Manabe and Stouffer (1979, 1980)		7
Hansen *et al.* (1984)[b]	6	
Hansen *et al.* (1984)	4	

[a] From U.S. Academy of Sciences (1982).
[b] No seasonal variation of insolation.

reaching the Earth's surface. In addition, the increase in the absolute humidity in the troposphere accompanied by the CO_2-induced warming also contributes to the increase in the downward flux of atmospheric radiation. Thus, a larger amount of radiative energy is received by the Earth's surface to be removed as turbulent fluxes of sensible and latent heat. This accounts for the increase in the global mean rate of evaporation.

One can identify another important factor that is responsible for the increase in the global mean evaporation rate. Following the Clausius–Clapeyron relationship, saturation vapor pressure increases almost exponentially with linear increase of temperature. This usually implies that surface-air difference in absolute humidity increases almost exponentially with a linear increase in the surface temperature. Thus, when the surface temperature is high, evaporation becomes a more effective means of ventilating the Earth's surface than the turbulent flux of sensible heat. Accordingly, a larger fraction of radiative energy received by the Earth's surface is removed as latent heat rather than sensible heat. Therefore, the rate of evaporation increases.

In order to balance the quasi-steady state of the model atmosphere, the increase in the area mean rate of evaporation should be matched by a similar increase of precipitation. This explains why the area mean rates of both evaporation and precipitation increase in response to an increase of atmospheric CO_2. For further discussion of the physical mechanisms for the intensification of the hydrologic cycle, see Manabe and Wetherald (1975) and Wetherald and Manabe (1975).

The global intensification of the hydrologic cycle due to an increase in atmospheric CO_2 is evident in Fig. 4, which illustrates the latitudinal distributions of annually averaged, zonal-mean rates of precipitation and evapo-

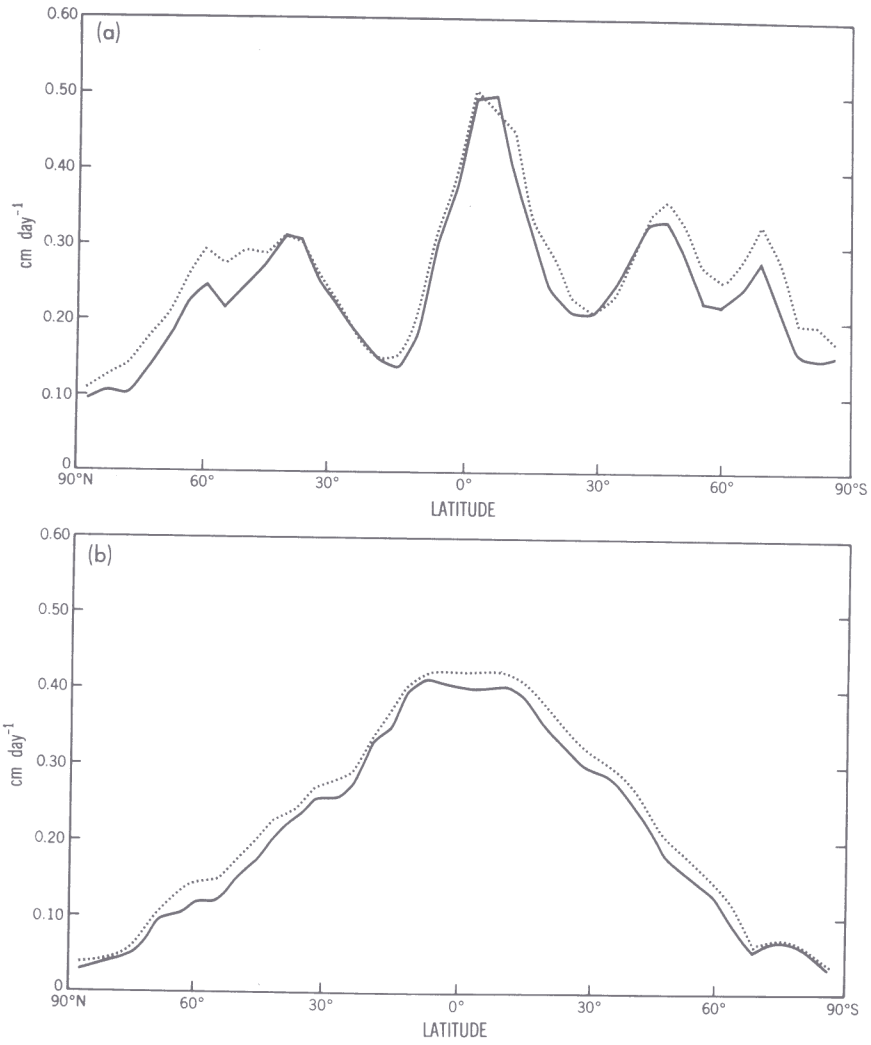

FIG. 4. Latitudinal distributions of annually averaged zonal mean rates of (a) precipitation and (b) evaporation. The results from the $4 \times CO_2$ and $1 \times CO_2$ experiments with the global model are indicated by dotted line and solid line, respectively. [From Manabe and Stouffer (1980). Reproduced with permission from *JGR, Journal of Geophysical Research* **85**(C-10), 5529–5554, copyright by the American Geophysical Union.]

ration from the global model with the normal ($1 \times CO_2$) and four times the normal ($4 \times CO_2$) concentration of the atmospheric CO_2. At high latitudes, the CO_2-induced increase in the precipitation rate is much larger than that of the evaporation rate. This result implies that the poleward moisture trans-

port in the $4 \times CO_2$ atmosphere is larger than the corresponding transport in the $1 \times CO_2$ atmosphere. The increase in the moisture content of air resulting from the CO_2-induced warming of the model troposphere accounts for the increase of the poleward moisture transport as discussed by Manabe and Wetherald (1980).

The CO_2-induced warming is particularly pronounced in the lower tropo-

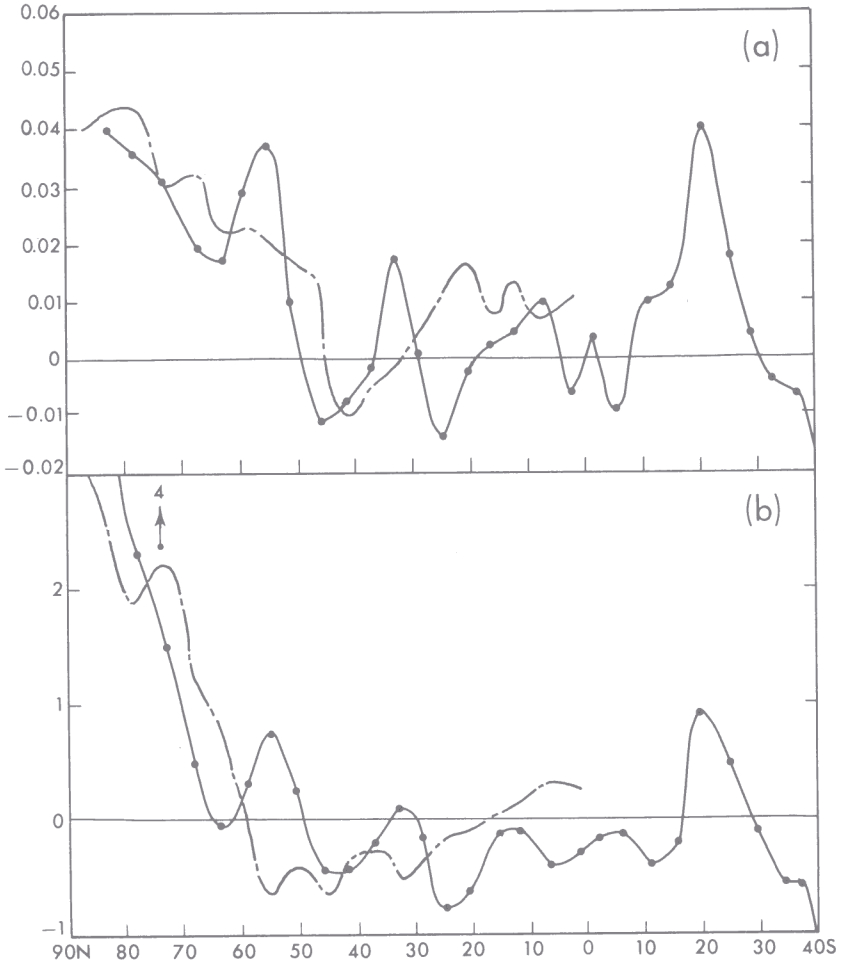

FIG. 5. Latitudinal distributions of the zonally averaged, annual-mean differences in (a) the rates of runoff (centimeters per day) and (b) soil moisture (centimeters) between the $4 \times CO_2$ and $1 \times CO_2$ experiment over the continents of the global model. The solid and dash-dotted lines illustrate the results from the global and sector model, respectively. The zonal averaging is done over the continents only.

sphere in high latitudes. This implies the penetration of warm, moisture-rich air into these latitudes, causing a large increase in precipitation rate. Therefore, both runoff rate and soil moisture also increase markedly in the Arctic and Subarctic regions of the global model. This is indicated in Fig. 5, which shows the latitudinal distributions of annually averaged, zonal-mean differences in the rate of runoff, and soil moisture between the $4 \times CO_2$ and $1 \times CO_2$ experiments. It is estimated that the rate of runoff in the global model, area-averaged over the continental regions poleward of 55°N, increases by as much as 45% in response to the quadrupling of the atmospheric CO_2 concentration. (The continental area chosen for this averaging includes most of the basins of the Siberian and Canadian rivers that flow into the Arctic Ocean.) Similar increases in both soil moisture and the rate of runoff also occur in the high latitudes of the sector model, as illustrated by Fig. 5.

In his recent review article, Schlesinger (1983) compared the distributions of the CO_2-induced changes in precipitation rate obtained from a wide variety of numerical experiments. With the exception of one experiment conducted under the assumption of fixed sea-surface temperature (Gates *et al.*, 1981), all experiments, including those performed by the present authors, indicate a relatively large increase in precipitation rate in high latitudes [see Figures 24 and 28 of Schlesinger (1983)]. Qualitative agreement among the results from these experiments suggests that this aspect of the CO_2-induced hydrologic change is particularly significant.

In Fig. 5, one also notes other CO_2-induced changes in zonally averaged, annual-mean soil moisture. For example, zonal-mean soil moisture reduces slightly in the middle latitudes and the subtropics of both models. In the tropics, zonal-mean soil moisture reduces for the global model, whereas it increases for the sector model. The discrepancy between the global and sector models in the tropics, suggests that the computed changes of soil moisture are not meaningful in this region. This speculation is consistent with the results of statistical significance tests that were conducted in Manabe *et al.* (1981).

4. Seasonal Response

This section evaluates how the CO_2-induced change in hydrology depends on seasons based on the results from both the sector and global models. Figures 6 and 7 contain the latitude–time distributions of the following variables from these two models:

(1) The difference in zonally averaged soil moisture between the $4 \times CO_2$ and $1 \times CO_2$ experiments (i.e., $\Delta[W]$).

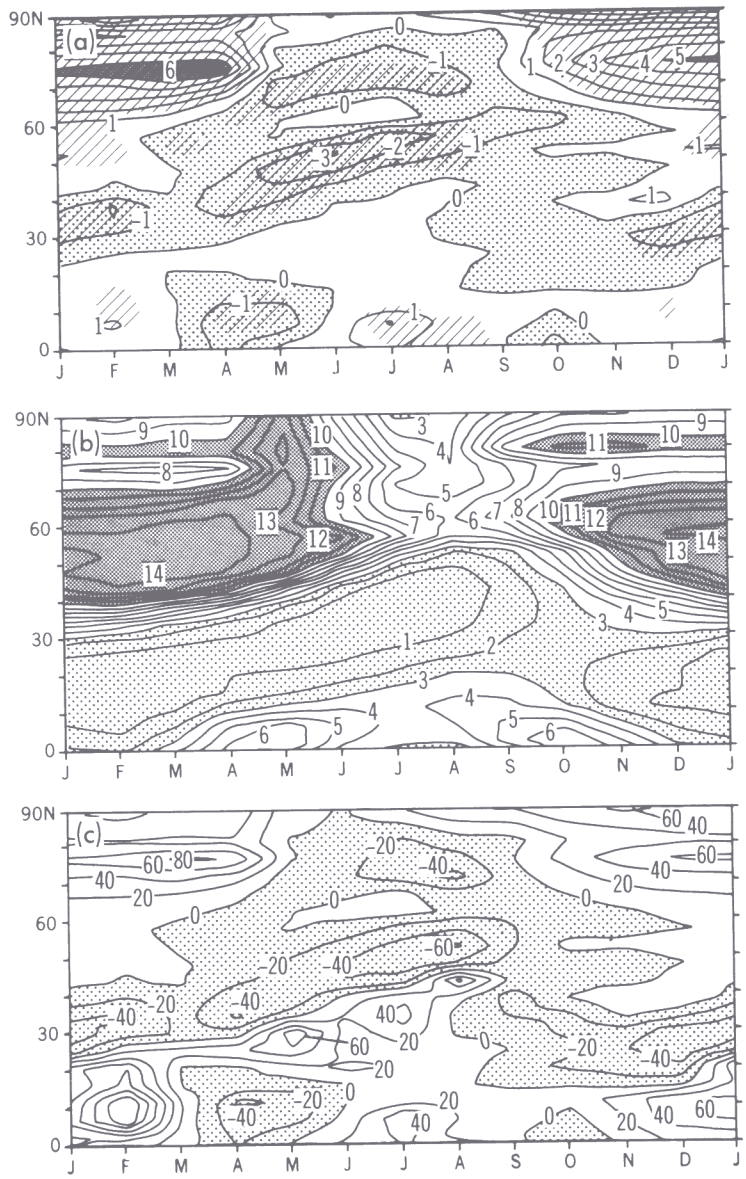

FIG. 6. The latitudinal and seasonal variation of (a) the difference of zonally averaged, monthly mean soil moisture (centimeters) between the $4 \times CO_2$ and the $1 \times CO_2$ experiment, (b) zonally averaged, monthly mean soil moisture from the $1 \times CO_2$ experiment, and (c) percentage change of the zonal-mean soil moisture from the $1 \times CO_2$ to the $4 \times CO_2$ experiment with the sector model. The zonal averaging is made over the continents. In (a) the areas identified by the shading of slant lines indicates the regions in which the soil moisture difference between the two experiments is statistically significant at or above 90% confidence level. [From Manabe *et al.* (1981).]

(2) The zonally averaged soil moisture from the $1 \times CO_2$ experiment (i.e., $[W]$).

(3) The fractional difference in zonally averaged soil moisture between the two experiments (i.e., $\Delta[W]/[W]$).

The distributions (2) and (3) are added to the figure for the assessment of the relative magnitude of the CO_2-induced change as compared with the original value of soil moisture. To evaluate the statistical significance of the results, the student t test is conducted. The slant-shaded areas in Figs. 6a and 7a indicate the zones where the CO_2-induced change of zonal-mean soil moisture is statistically significant at or above the 90% confidence level.

Although the idealized geography of the sector model is quite different from the realistic geography of the global model, one can identify several common characteristics in the distribution of the CO_2-induced change of soil moisture obtained from these two models. For example, the difference in soil moisture in high latitudes has a large positive value throughout most of the year with the exception of the summer season. As discussed in the preceding section, this CO_2-induced increase of soil moisture results from penetration of warm, moisture-rich air into the high latitudes of the model. One also notes two zones of reduced soil wetness at the middle and high latitudes during the summer season. In addition, a large fractional reduction of zontal-mean soil moisture is indicated at about 25°N during winter. These changes in soil moisture are statistically significant at or above the 90% confidence level. It is therefore worthwhile to explore the physical mechanisms responsible for these CO_2-induced changes of soil moisture.

To determine the mechanisms responsible for the CO_2-induced summer dryness in the middle and high latitudes described in the preceding, Manabe *et al.* (1981) made an extensive analysis of the seasonal variation of soil moisture budget obtained from the model experiments. Their analysis reveals that, in high latitudes, the CO_2-induced summer dryness results mainly from the change in the timing of the snowmelt season when soil is usually saturated with water. After the disappearance of snow cover, the rate of evaporation becomes very large and the depletion of soil moisture becomes very rapid because of marked reduction in surface albedo and increased surface absorption of insolation. Since the snowmelt season in the $4 \times CO_2$ experiment ends earlier than the corresponding season in the $1 \times CO_2$ experiment, the warm season of rapid soil moisture depletion begins earlier, resulting in less soil moisture in summer in the $4 \times CO_2$ experiment.

With the exception of the summer season, soil moisture in high latitudes increases in response to the increase of CO_2 concentration in the atmosphere. In the $4 \times CO_2$ experiment, a larger fraction of high-latitude precipitation occurs as rainfall during the late fall and early winter because of higher

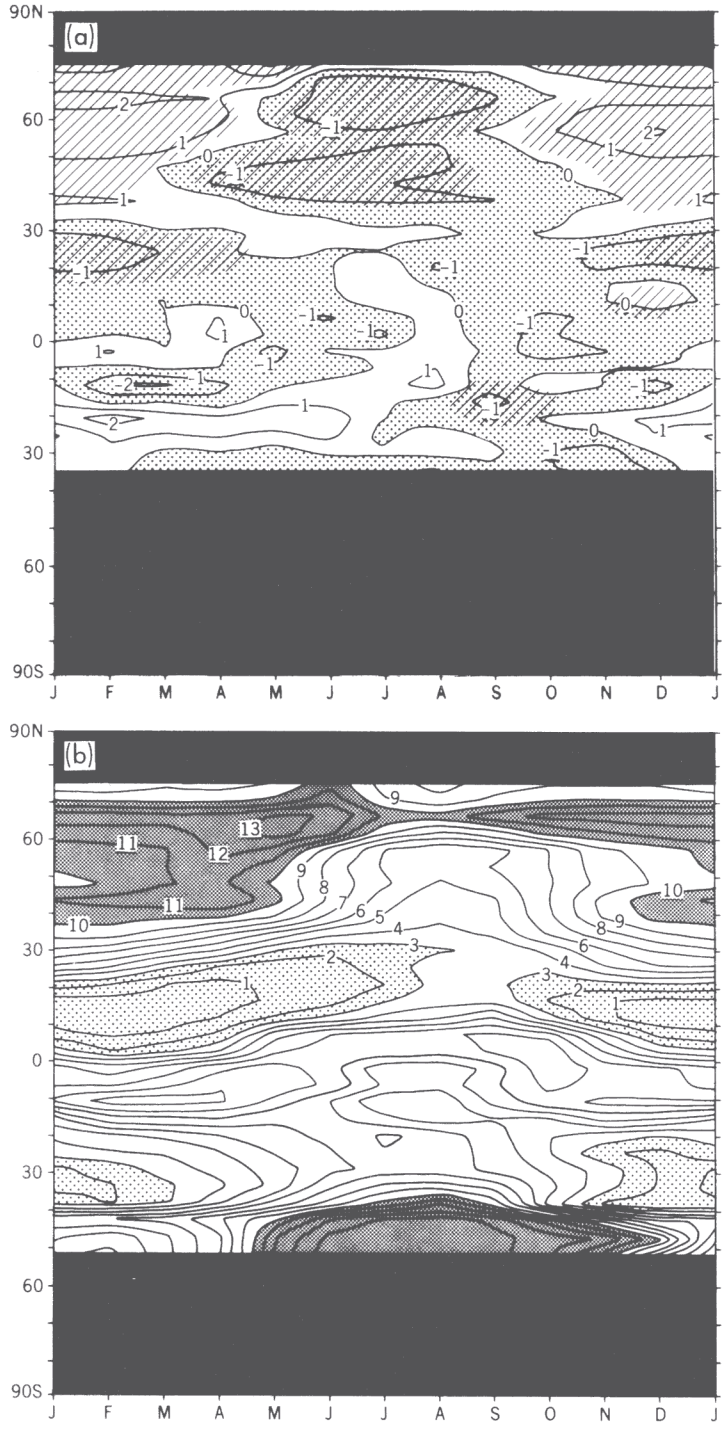

FIG. 7. Same as Fig. 6, except that the results are obtained by use of the global model.

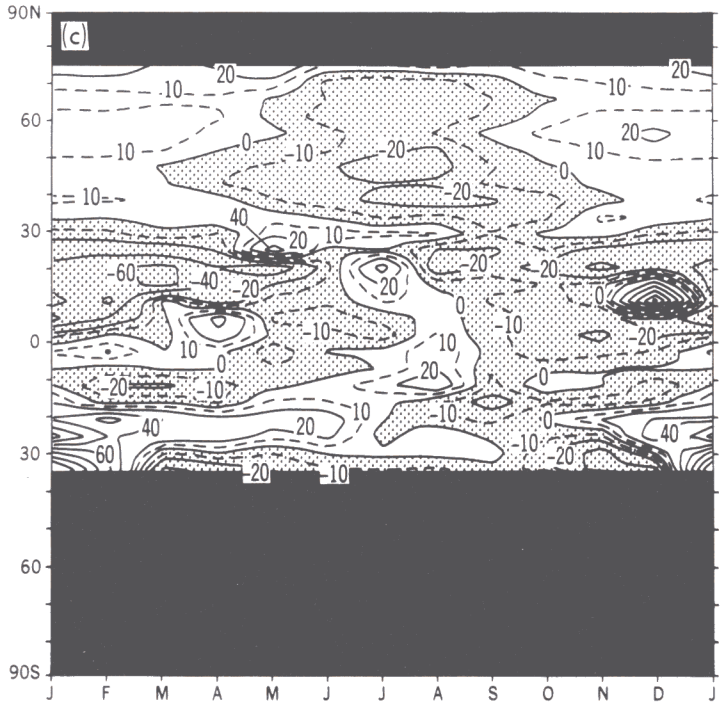

FIG. 7. *(continued)*

surface-air temperatures. This is why the high latitude storage of soil moisture in the $4 \times CO_2$ experiment is larger than that of the $1 \times CO_2$ experiment during the late fall and remains at a high level throughout the winter when snow cover prevents the evaporative reduction of soil moisture.

In the middle latitudes, the earlier timing of the spring maximum in snowmelt also contributes to the summer dryness as it does in the high latitudes. In addition, the CO_2-induced poleward shift of the mid-latitude rainbelt also helps induce the summer dryness. In the CO_2-rich, warm climate, the mid-latitude rainbelt is located poleward of the corresponding rainbelt in the normal CO_2 climate because of the penetration of moist and warm air masses into higher latitudes. For example, this poleward shift is evident in a later figure (Fig. 9a), which illustrates the latitudinal profile of winter precipitation from the sector model. In the annual mean profile of precipitation rate from the global model shown in Fig. 4a, the latitude of maximum precipitation rate hardly changes in response to the CO_2-increase. The shift, however, manifests itself as an asymmetric increase in precipitation rate relative to the latitude of maximum precipitation rate (i.e., the CO_2-induced increase in the zonal belt located poleward of the maximum is

larger than the corresponding increase in the region located equatorward of the maximum). Figure 8 schematically illustrates the impact of this poleward shift on soil wetness. This figure indicates that, at the latitude identified by the thin zonal line, the spring transit of the mid-latitude rainbelt in the $4 \times CO_2$ experiment occurs earlier than the corresponding transit in the $1 \times CO_2$ experiment. Accordingly, the spring to summer reduction in precipitation rate occurs earlier. Since the soil in most regions of the middle latitudes is often saturated with water in spring for both experiments, this implies that the soil is dryer during summer in the $4 \times CO_2$ as compared with the $1 \times CO_2$ experiment.

One can identify another factor that contributes to the summer dryness in the middle latitudes. In the $4 \times CO_2$ experiment, the summer period of weak storminess begins earlier and ends later than the corresponding period in the

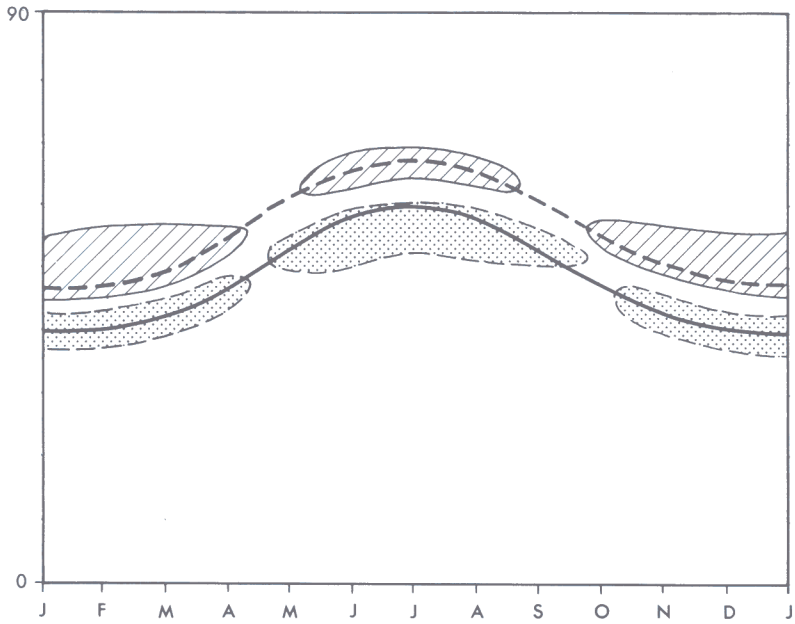

FIG. 8. Schematic diagram illustrating the change in soil wetness that results from the poleward shift of the middle-latitude rainbelt. Solid and dashed lines indicate the positions of the middle-latitude rainbelt in the $1 \times CO_2$ and $4 \times CO_2$ experiment, respectively. Stippled and cross-hatched areas indicate the areas of reduced and increased soil moisture, respectively. In addition to the poleward shift of the latitudinal profile of precipitation rate in the middle latitudes, other changes occur in the distribution of both precipitation and evaporation. The influences of these CO_2-induced changes on soil wetness are not taken into consideration in this schematic diagram.

standard experiment. It is expected that this feature helps reduce soil moisture during the summer season (Manabe *et al.,* 1981).

The possibility of summer reduction of soil moisture in the middle latitudes is also suggested by Mitchell (1983) on the basis of the results from some of his numerical experiments. However, the recent results by Washington and Meehl (1984) fail to indicate a similar CO_2-induced change of soil moisture. A comparative analysis of these results is required in order to determine the cause of the discrepancy.

By reversing the discussion of the relationship between the poleward shift of the middle-latitude rainbelt and the CO_2-induced summer dryness, one can identify the mechanism for the CO_2-induced winter wetness in the middle latitudes that is evident in Figs. 6 and 7. This is illustrated in the schematic diagram of Fig. 8 in which the regions of increased wetness are indicated by slanted shade. For the more rigorous discussion of the CO_2-induced change of soil moisture, refer to the study by Manabe *et al.* (1981) in which both the annual and seasonal components of soil moisture budget are examined.

Another important consequence of the CO_2-induced shift of the mid-latitude rainbelt is the enhanced dryness in the subtropics during winter. This enhanced winter dryness is indicated at about 35° latitude in Fig. 6 (from the sector model) and around 25°N in Fig. 7 (from the global model). It is also illustrated schematically in Fig. 8.

In order to evaluate the mechanism for this CO_2-induced winter dryness, Fig. 9 is constructed. This figure compares the latitudinal distributions of the rates of precipitation P, evaporation E, and $P - E$ during the December–January–February period obtained from both the $4 \times CO_2$ and $1 \times CO_2$ experiments conducted by the use of the sector model. According to this figure, the poleward shift of the mid-latitude rainbelt reduces $P - E$ and runoff equatorward of the latitude of maximum precipitation rate. In winter when the mid-latitude rainbelt is located at its lowest latitude, this $P - E$ reduction occurs in the subtropical latitudes and contributes to the winter dryness of soil, as illustrated in Fig. 8.

The winter dryness in the subtropics is evident in the results of Manabe *et al.* (1981) and was briefly noted in the review paper by Manabe (1983). However, this is the first article in which the physical mechanism responsible for this phenomenon is extensively discussed. A poleward shift of the middle-latitude rainbelt was also found to be responsible for a zonal belt of increased soil dryness in the middle latitudes of a model with the annual-mean insolation [see Figs. 13 and 14 in the paper by Manabe and Wetherald (1980)].

In order to appreciate the practical implication of the CO_2-induced change

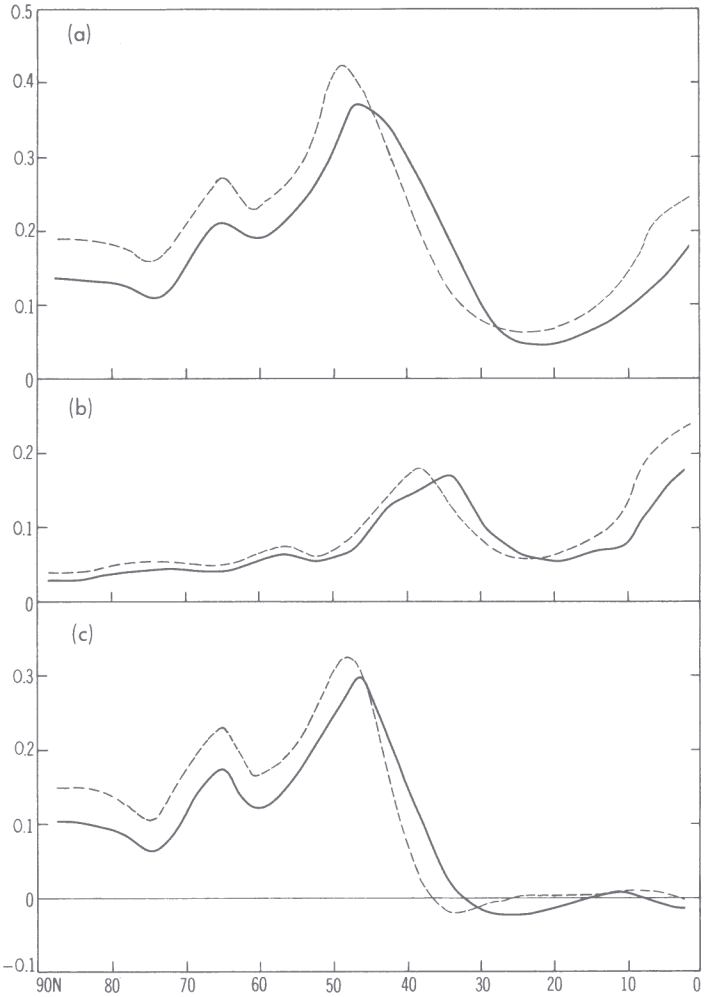

FIG. 9. Latitudinal distributions of the zonal-mean rates of (a) precipitation, (b) evaporation, and (c) precipitation minus evaporation in the continents of the sector model averaged over the three winter months. The zonal averaging is made over the continents. Solid and dashed lines indicate results from the $1 \times CO_2$ and $4 \times CO_2$ experiment, respectively.

of soil moisture described in this section and assess its detectability, one can compare this change with the natural variability of soil moisture by computing the signal-to-noise ratio S/N, defined by

$$S/N = \Delta_c[W]/\sigma_{[W]}$$

where $\Delta_c[W]$ and $\sigma_{[W]}$ are the CO_2-induced change and the standard deviation of zonally averaged soil moisture, respectively.

Manabe and Stouffer (Manabe, 1983) computed the latitudinal and seasonal variation of the signal-to-noise ratio for the CO_2-induced change of zonally averaged soil moisture obtained from the global model. Their results are illustrated in Fig. 10. As expected, the features with relatively high statistical significance also have a high signal-to-noise ratio. These features include the enhanced summer dryness in the middle and high latitudes of the Northern Hemisphere, the enhanced winter dryness around 25°N, and the increased wetness around 60°N during the fall–winter–spring period. The signal-to-noise ratios for these CO_2-induced changes are about two, implying that their magnitude is comparable with the amplitude of natural variability of zonal-mean soil moisture. These ratios may be compared with the signal-to-noise ratio for the CO_2-induced change in zonally averaged surface-air temperature, which ranges from 5 to 20 [see Manabe (1983)]. This result

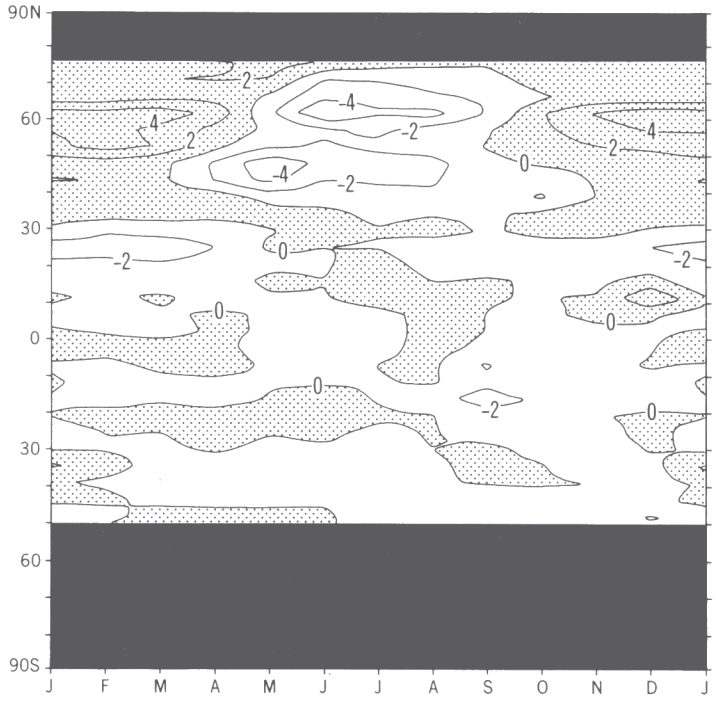

FIG. 10. The latitude–time distribution of the signal-to-noise ratio for the change of zonally averaged, monthly mean soil moisture over continents of the global model in response to the quadrupling of atmospheric CO_2 concentrations. [From Manabe (1983).]

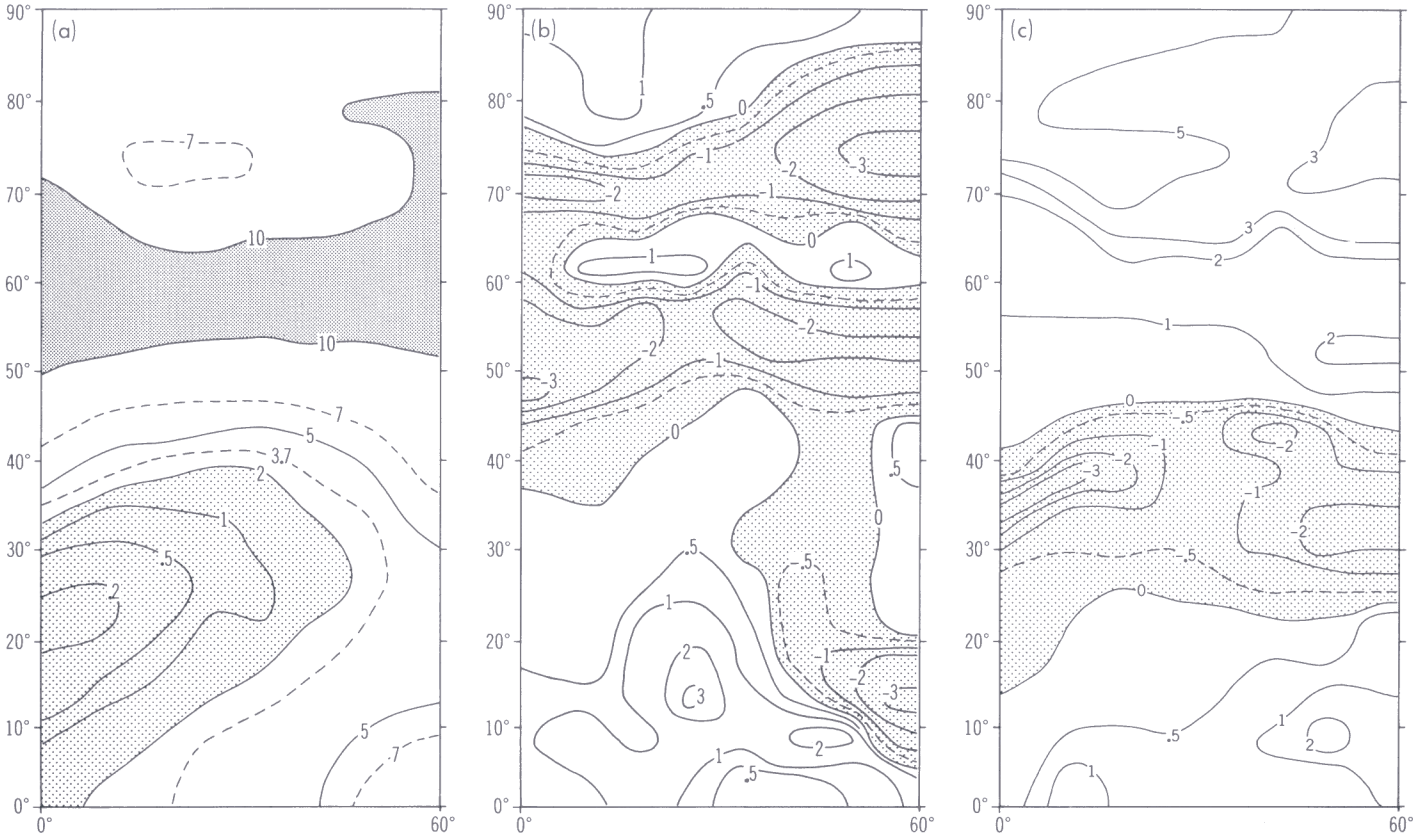

FIG. 11. Sector model distributions of (a) annual-mean soil moisture (centimeters) from the $1 \times CO_2$ experiment, (b) the soil moisture difference (centimeters) between the $4 \times CO_2$ and $1 \times CO_2$ experiment averaged over the three summer months, and (c) corresponding difference averaged over the three winter months. Note that only the distributions over the model continent are illustrated.

suggests that it is much harder to detect the CO_2-induced change of soil moisture than that of surface-air temperature.

So far, only the CO_2-induced changes in zonally averaged distribution of hydrological variables have been discussed. However, it is of particular interest to examine the geographical distributions of the CO_2-induced changes. Unfortunately, the geographical distribution of CO_2-induced hydrologic changes is obscured by the noise due to the natural variability of model hydrology. Therefore, it is often very difficult to distinguish these two from one another. Under these circumstances, the results from the sector model with simple geography are discussed first, followed by the evaluation of the results from the global model with realistic geography.

Figure 11 illustrates the geographical distributions of the CO_2-induced change in soil moisture obtained from the sector model for two seasons of a year. In addition, the geographical distribution of the annual-mean soil moisture itself is added to the same figure for reference. During the winter season, soil moisture reduces along the northern periphery of a subtropical desert (compare Fig. 11c with Fig. 11a). As discussed earlier, the poleward shift of the mid-latitude rainbelt is responsible for this CO_2-induced dryness in the subtropics. In a steppe region located at the poleward periphery of a subtropical desert, significant precipitation occurs only during winter, i.e., the period when the mid-latitude rainbelt is located at its lowest latitude. It is expected that this winter precipitation reduces in response to the CO_2-induced poleward shift of the mid-latitude rainbelt. Therefore, soil moisture reduces substantially during winter in the arid steppe located in the poleward periphery of the subtropical desert.

Figure 11c also indicates that, during winter, soil moisture increases significantly in high latitudes. As discussed already, this partly results from the increase in the fraction of precipitation that occurs as rainfall during the late fall and early winter. Furthermore, precipitation itself increases markedly in high latitudes in response to the increase of atmospheric carbon dioxide because of the penetration of moisture-rich air into the polar regions.

In the summer season, one can identify in Fig. 11b the two belts of reduced soil moisture in the middle and high latitudes. The mechanisms responsible for causing these double belts of reduced dryness were already discussed. The mid-latitude dryness extends the subtropical region of low soil moisture into higher latitudes in summer. This statement may be confirmed by referring to Fig. 6, which illustrates the zonally averaged soil moisture and its CO_2-induced change.

The results from the global model are illustrated in Fig. 12. As was the case in Fig. 11, the distribution of annual-mean soil moisture is added to the top portion of the figure for reference. This figure indicates that the global model successfully reproduces the region of low soil moisture in the Sahara, Gobi,

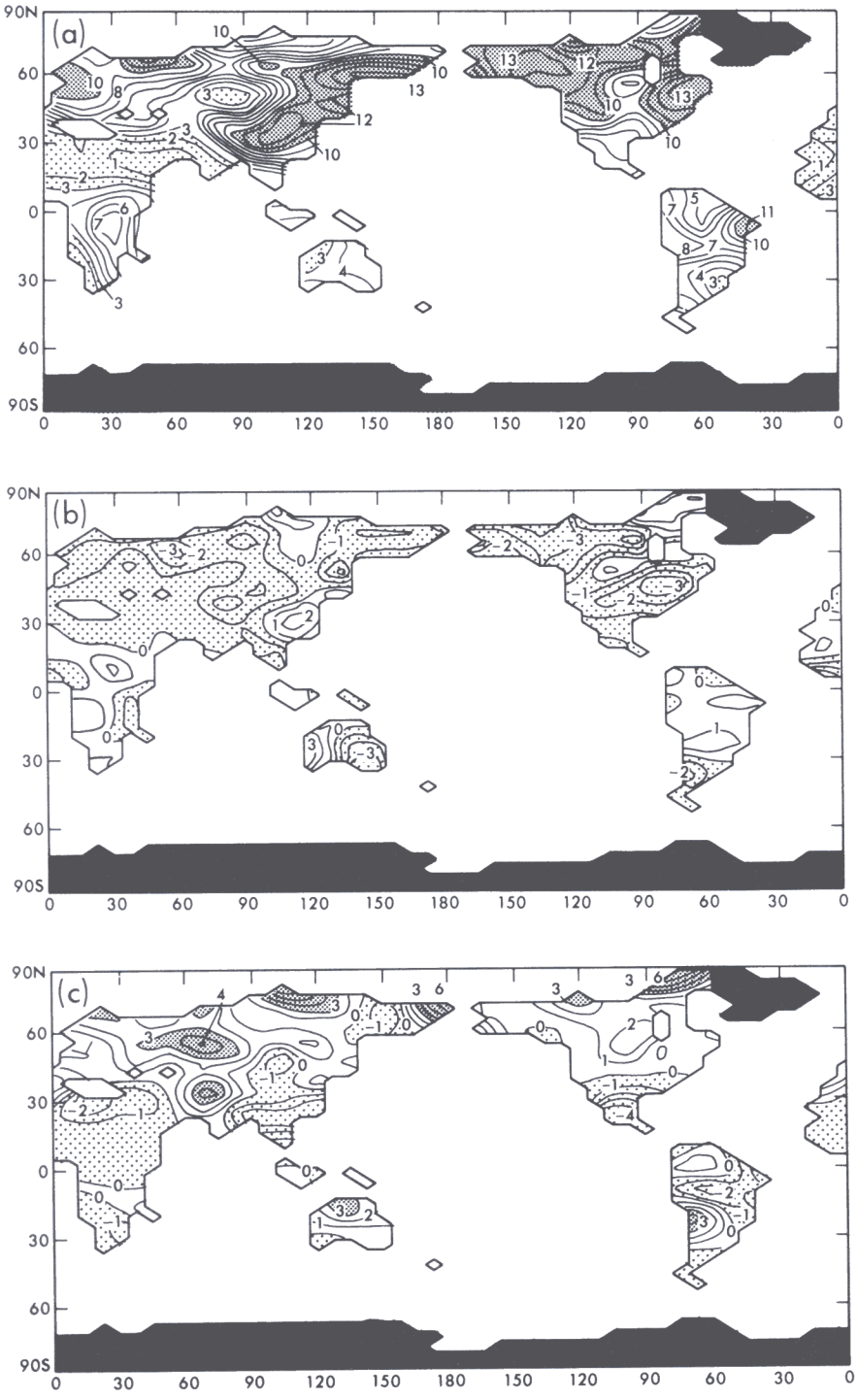
(a)
(b)
(c)
90N
60
30
0
30
60
90S
0 30 60 90 120 150 180 150 120 90 60 30 0

and Kalahari Deserts. However, it appears that soil moisture in Australia and the southwestern part of the United States is overestimated.

In Fig. 12c, which illustrates the geographical distribution of the CO_2-induced change of soil moisture during the period of December–January–February, one notes an extensive belt of reduced soil moisture along the northern periphery of the Sahara Desert. This is in qualitative agreement with the results from the sector model described earlier. However, Figs. 12b and 12c indicate that soil moisture does not necessarily reduce in other subtropical deserts with a smaller scale such as those in the Southern hemisphere. As discussed next, these small-scale changes of soil moisture are not statistically significant.

In high latitudes of the global model, i.e., over Siberia and Canada, one can identify extensive regions of increased soil wetness during winter (Fig. 12c) in qualitative agreement with the results from the sector model. Another feature of interest in Fig. 12b is the summer reduction of soil moisture in the middle and high latitudes over the North American and Eurasian continents. It is encouraging that this feature of the soil moisture reduction in the global model also resembles the CO_2-induced summer dryness pattern in the sector model described earlier. However, it is desirable to confirm that the mechanism for inducing the summer dryness of the zonally averaged soil moisture also causes the regional summer dryness over both the North American and Eurasian continents.

In the geographical distribution of the CO_2-induced change of soil moisture illustrated in Figs. 12b and 12c, one notes many small-scale changes of soil moisture in the tropics and the Southern Hemisphere. However, one should not take these changes too literally in view of (1) the low statistical significance of these details and (2) the failure of the climate model to simulate some of the small-scale changes in the observed geographical distributions of hydrologic variables. Further improvement of the climate model is required before one can determine with confidence the small-scale features of the CO_2-induced hydrologic change and investigate how it is related to the zonally averaged change discussed earlier. In addition, it is desirable to extend the period of numerical time integration of a model in a climate sensitivity experiment in order to obtain a result with higher statistical significance.

FIG. 12. Global model distributions of (a) annual-mean soil moisture (centimeters) from the $1 \times CO_2$ experiment, (b) the soil moisture difference (centimeters) between the $4 \times CO_2$ and $1 \times CO_2$ experiment averaged over the three summer months, and (c) corresponding difference averaged over the three winter months.

5. Concluding Remarks

Based on the results from a series of numerical experiments with climate models, it has been suggested that an increase in atmospheric CO_2 not only alters the atmospheric temperature but also has a profound influence on the global hydrology. The hydrologic changes include (1) an increase in the global-mean rates of both precipitation and evaporation, (2) a particularly large increase in annual-mean rate of runoff in high latitudes, (3) earlier arrival of the snowmelt season, (4) enhanced summer dryness in middle and high latitudes, (5) increased soil moisture in middle and high latitudes during the colder half of the year, and (6) a winter reduction of soil moisture in the poleward periphery of a subtropical desert. The physical mechanisms that cause these hydrologic changes in climate models are discussed.

In the mathematical models of climate that were used in the studies discussed in this article, the distribution of cloud cover is prescribed. If cloud cover is allowed to change, the CO_2-induced hydrologic changes could have been different from those identified here. Nevertheless, it is encouraging that the preliminary results from a GFDL model with predicted cloud cover include the hydrologic changes that are qualitatively similar to these changes. However, a prognostic scheme of cloud cover is at an early stage of development. The difficulty in developing a reliable parameterization of the cloud-radiation feedback process is one of major sources of uncertainty in the current assessment of climate sensitivity. This is why the World Climate Research Program places an increasing emphasis on the improvement of such a parameterization as manifested in the International Satellite Cloud Climatology Project.

Most of the hydrologic changes discussed here are either globally averaged or zonally averaged changes. Unfortunately, it has been very difficult to determine the detailed geographical distribution of the CO_2-induced hydrologic changes for the following reasons. First, the hydrologic states as simulated by a model undergo large temporal fluctuations, particularly in arid regions. Therefore, it is necessary to conduct the numerical time integration of the model with normal and high CO_2 concentrations over a very long period of time in order to distinguish the signals of CO_2-induced changes from the noise of natural hydrologic variability. This requires a very large amount of computer time. The second reason stems from the fact that the current simulations of the geographical distributions of hydrologic variables are far from satisfactory. The geographical details of the CO_2-induced climate change obtained from numerical experiments should be regarded with caution until a further improvement is achieved in the simulation of the observed climate.

One should also note that the atmosphere–mixed layer ocean models discussed in this article do not include oceanic heat transport. The study of Spelman and Manabe (1984) clearly indicates profound effects of oceanic heat transport on climate and hydrology. For the successful simulation of the geographical distribution of climate, it is therefore necessary to use a coupled ocean–atmosphere model in which the effect of oceanic heat transport is taken into consideration. Unfortunately, the currently available coupled models cannot simulate satisfactorily the global distribution of water mass and accordingly the heat exchange between the atmosphere and oceans. At the Geophysical Fluid Dynamics Laboratory of the National Oceanic and Atmospheric Administration (NOAA), continuous effort has been made for the improvement and validation of the ocean circulation model. For example, Sarmiento and Bryan (1982) and Sarmiento (1983) attempted to simulate the temporal and spatial variation of tritium released from nuclear weapon tests. The transient tracer experiment, which monitors various trace materials (including tritium) in the world oceans, will continue to provide ideal data for the validation of an ocean model. In addition, a plan is being developed for an ambitious observational program of the world oceans, i.e., the World Ocean Circulation Experiment. It is expected that the program will yield valuable data for model verification.

In this article, the CO_2-induced change of climate is investigated by comparing two climates of a model with the normal and above-normal concentration of carbon dioxide. In other words, the present article evaluates the total equilibrium response of a model climate to a CO_2 forcing exerted over an infinite length of time. The present authors believe that the physical processes that control this equilibrium response of hydrology also control the transient response of hydrology to a future increase in the atmospheric carbon dioxide. However, it is likely that the geographical details of the equilibrium and the transient response may be quantitatively different from each other because of spatial variation of the effective thermal inertia of the atmosphere–continent–ocean system (Schneider and Thompson, 1981). In order to investigate this issue, it is again necessary to use a coupled ocean–atmosphere model in which the thermal inertia of a full ocean is properly taken into consideration. Although a preliminary study of this kind has been conducted by Bryan *et al.* (1982) and Spelman and Manabe (1984), it has not investigated the hydrologic aspect of the transient response.

Fortunately, the recent advancement of computer technology has made it possible for the first time to perform a time integration of a coupled ocean–atmosphere model over a sufficiently long period of time. Furthermore, various global observational programs of oceans and atmosphere, which are currently planned by international oceanographic and climate research

communities, can yield valuable data for the improvement of a coupled model. Therefore, it is expected that vigorous studies of transient and equilibrium response of climate will begin by use of a model in which a general circulation model of oceans is coupled with that of the atmosphere.

References

Bryan, K., Komro, F. G., Manabe, S., and Spelman, M. J. (1982). Transient climate response to increasing atmospheric CO_2. *Science* **215,** 56–58.

Callender, G. S. (1938). The artificial production of carbon dioxide and its influence on temperature. *Q. J. R. Meteorol. Soc.* **64,** 223–240.

Gates, W. L., Cook, K. H., and Schlesinger, M. E. (1981). Preliminary analysis of experiments on the climatic effects of increasing CO_2 with an atmospheric general circulation model and a climatological ocean model. *J. Geophys. Res.* **86,** 6385–6393.

Hansen, J., Lacis, A., Russel, G., Stone, P., Fung, I., Ruedy, R., and Lerner, J. (1984). Climate sensitivity: Analysis of feedback mechanisms. *In "Climate Process and Climate Sensitivity"* (J. E. Hansen and T. Takahashi, eds.), Maurice Ewing Series no. 5, 130–163.

Manabe, S. (1982). Simulation of climate by general circulation models with hydrologic cycle. *In* "Land Surface Process in Atmospheric General Circulation Model" (P. S. Eagleson, eds.), 19–66. Cambridge Univ. Press, London and New York.

Manabe, S. (1983). Carbon dioxide and climatic change in theory of climate. *Adv. Geophys.* **20,** 39–82.

Manabe, S., and Stouffer, R. J. (1979). A CO_2-climate sensitivity study with a mathematical model of the global climate. *Nature (London)* **282,** 491–493.

Manabe, S., and Stouffer, R. J. (1980). Sensitivity of a global model to an increase of CO_2-concentration in the atmosphere. *JGR, J. Geophys. Res.* **85** (C-10), 5529–5554.

Manabe, S. and Wetherald, R. T. (1975). The effect of doubling the CO_2-concentration of the climate of a general circulation model. *J. Atmos. Sci.* **32,** 3–15.

Manabe, S., and Wetherald, R. T. (1980). On the distribution of climate change resulting from an increase in CO_2-content of the atmosphere. *J. Atmos. Sci.* **37,** 99–118.

Manabe, S., Smagorinsky, J., and Strickler, R. F. (1965). Simulated climatology of a general circulation model with a hydrologic cycle. *Mon. Weather Rev.* **93,** 769–798.

Manabe, S., Wetherald, R. T., and Stouffer, R. J. (1981). Summer dryness due to an increase of atmospheric CO_2-concentration. *Clim. Change* **3,** 347–386.

Mitchell, J. F. B. (1983). The seasonal response of a general circulation model to changes in CO_2 and sea temperatures. *Q. J. R. Meteorol.* **109,** 113–152.

Sarmiento, J. L. (1983). A simulation of bomb tritium entry into the Atlantic Ocean. *J. Phys. Oceanogr.* **13,** 1924–1939.

Sarmiento, J. L., and Bryan, K. (1982). An ocean transport model for the North Atlantic. *JGR, J. Geophys. Res.* **87**(C1), 394–408.

Schlesinger, M. E. (1983). Simulating CO_2-induced climate change with mathematical climate models: Capabilities, limitations, and prospects. *In* "Proceedings of the Conference on Carbon Dioxide, Climate, and Consensus," Vol. III, pp. 3–140. U.S. Dept. of Energy, Washington, D.C.

Schneider, S. H., and Thompson, S. L. (1981). Atmospheric CO_2 and climate: Importance of the transient response. *JGR, J. Geophys. Res.* **86**(C4), 3135–3147.

Smagorinsky, J. (1956). On the inclusion of moist adiabatic process in numerical weather prediction models. *Ber. Dtsch. Wetterdienstes* No. 38, 82–90.

Spelman, M. J., and Manabe, S. (1984). Influence of oceanic heat transport upon the sensitivity of a model climate. *JGR, J. Geophys. Res.* **89**(C1), 571–586.

U.S. National Academy of Sciences (1982). "Carbon Dioxide and Climate: A Second Assessment." Natl. Acad. Press, Washington, D.C.

U.S. National Academy of Sciences (1983). "Changing Climate." Natl. Acad. Press, Washington, D.C.

Washington, W. M., and Meehl, J. (1984). Seasonal cycle experiments on the climate sensitivity due to a doubling of CO_2 with an atmospheric general circulation model coupled to a simple mixed layer ocean model. *JGR, J. Geophys. Res.* **89**(D6), 9475–9503.

Wetherald, R. T., and Manabe, S. (1975). The effect of changing solar constant on the climate of a general circulation model. *J. Atmos. Sci.* **32,** 2044–2059.

Wetherald, R. T., and Manabe, S. (1981). Influence of seasonal variation upon the sensitivity of a model climate. *JGR, J. Geophys. Res.* **86,** 1194–1204.